Solar Phys (2008) 252: 55–71
DOI 10.1007/s11207-008-9236-2

Lorentz Force: A Possible Driving Force for Sunspot Rotation

Jiangtao Su · Yu Liu · Jihong Liu · Xinjie Mao · Hongqi Zhang · Hui Li · Xiaofan Wang · Wenbin Xie

Received: 9 October 2007 / Accepted: 13 June 2008 / Published online: 29 July 2008

Abstract Zhao and Kosovichev (*Astrophys. J.* **591**, 446, 2003) found two opposite subphotospheric vortical flows in the depth range of 0 – 12 Mm around a fast rotating sunspot. So far there is no theoretical model explaining such flow motions. In this paper, we try to explain this phenomenon from the point of view of magnetic flux tubes interacting with large-scale vortical motions of plasma. In the deeper zone under the photosphere, the magnetic force may be less than the nonmagnetic force of plasma. The vortical flow located there twists the flux tube and magnetic free energy is built up in the tube. In the shallower zone under the photosphere, the magnetic force may be greater than the nonmagnetic force. Thus, part of the stored magnetic free energy is released to drive the plasma to rotate in two opposite directions, *e.g.*, in the depth ranges of 0 – 3(5) and 9 – 12 Mm. In addition, we also define a vector of nonpotential magnetic stress τ, which can be related to flare occurrence. It is calculated for the active region NOAA 10930 on 11 December 2006. We find that: *i*) the integral of its line-of-sight (LOS) stress successively increases around the magnetic neutral line (MNL) prior to and during the flare and decreases to a minimum after the flare; *ii*) the integral of its transverse stress exceeds the integral of its LOS component by one order of magnitude over the whole field of view; *iii*) the transverse stress first points toward the MNL, then along it, and finally it points away from it. We need other data to verify whether or not

J. Su (✉) · H. Zhang · X. Wang · W. Xie
National Astronomical Observatories, Chinese Academy of Sciences, Beijing 100012, China
e-mail: sjt@bao.ac.cn

Y. Liu
Institute for Astronomy, University of Hawaii, 2680 Woodlawn Drive, Honolulu, HI 96822, USA

J. Liu
Department of Physics, Shi Jiazhuang University, Shi Jiazhuang 050081, China

X. Mao
Astronomy Department, Beijing Normal University, Beijing 100875, China

H. Li
Purple Mountain Observatory, Chinese Academy of Sciences, Nanjing 210008, China

the magnetic energy is transported in the horizontal direction to the neutral line, and then partly changes into the energy in LOS direction before and during the flare.

Keywords Sun, convection · Magnetic fields · Magnetic force

1. Introduction

Sunspots that exhibit some degree of rotational motion around their own vertical axes are not rare in solar observations (Knoška, 1975). It is widely believed that the emergence of a twisted flux tube from the convection zone will give the appearance of rotation at the photosphere. A good example of sunspot rotation is the fast emerging flux region NOAA 10488, in which one magnetic flux system emerged from the sub-photosphere first showing significant footpoint rotation and two new magnetic flux systems emerged later exhibiting strong shear motions relative to the old flux system (Liu and Zhang, 2006). The origin of the magnetic twists observed in vector magnetograms and coronal loop structures may come from the solar differential rotation, surface motions and turbulent motions in the solar convection zone (Canfield and Pevtsov, 2000).

López Fuentes *et al.* (2003) suggested that there are three possible origins for the rotation of a sunspot. The first one is the nonlinear development of a kink-instability at the base of the convective zone; this would imply the formation of a nonplanar flux tube, while emerging across the photosphere, would show a rotation of its photospheric polarities as observed. The second one is the action of the Coriolis force as the flux tube travels through the convection zone. The last one is due to the interaction of flux tubes with large-scale vortical motions of the plasma in the convection zone, including also photospheric or shallow sub-photospheric large scale flows. Zhao and Kosovichev (2003) applied the method of time – distance helioseismology to a fast rotating sunspot and derived for the first time the subsurface vortical flow fields. Their study supports the argument by López Fuentes *et al.* (2003) that vortical flows may exist in sub-photosphere and play an important role in the formation of magnetic twists.

In the convection zone, due to the high plasma β value, the nonmagnetic forces should be much greater than the magnetic forces. However, in the region near or above the photosphere, the magnetic forces might be greater than the others and they can drive the plasma toward a state of minimum magnetic energy. Longcope and Welsch (2000) presented a dynamical model that connects a twisted sub-photospheric flux tube to a force free coronal field. The simplest observable prediction of this model is that the coronal twist will appear to increase for a period, which will accompany a rotation of the footpoints driven by magnetic forces in the twisted flux tube. Moreover, Manchester (2001) and Manchester *et al.* (2004) simulated the emergence of a flux rope and found that its two sides move in opposite directions as the flux rope expands. The motions of the flux rope are driven by magnetic forces. In the observations, Zhao and Kosovichev (2003) found opposite vortical flows in the depth range of 0 – 12 Mm around a sunspot.

In this paper, we try to qualitatively study this phenomenon in terms of the interaction of magnetic forces and sub-photospheric plasma. From a simplified sunspot model, we derive the formulae for calculating the Lorentz force (LF: F_x, F_y and F_z) acting on a part of the model sunspot. It is found that below the photosphere there should be two opposite magnetic torques created in a section of the twisted flux tube. As this partial flux tube emerges across the photosphere, the magnetic torques may drive the plasma to rotate oppositely at its two ends. A theoretical analysis of the relationship between magnetic tension and plasma is presented in Section 2, and in Section 3, we introduce the observing instruments and the observed data for a rotating sunspot. Section 4 outlines the observed results, and in Section 5 some discussions are presented.

2. A Qualitative Analysis of the LF on a Sunspot

2.1. An Untwisted Sunspot Model

The integral equation of motion for incompressible magnetic fluid is

$$\int_D \rho \frac{\mathrm{d}\boldsymbol{V}}{\mathrm{d}t}\,\mathrm{d}^3 r = \int_S \left[\frac{1}{\mu_0}\boldsymbol{BB} - \left(p + \frac{1}{2\mu_0}B^2\right)\boldsymbol{II}\right]\mathrm{d}S + \int_D \rho \boldsymbol{g}\,\mathrm{d}^3 r, \tag{1}$$

where D is the integral volume bounded by a surface S and $\boldsymbol{II}$ is the unit tensor. This equation can be used to analyze the forces acting on the flux tubes of a sunspot, of which we mainly discuss the possible roles of the LF on the motions of a sunspot. The integration of the first term on the right-hand side can be carried out over the surface of the sunspot. A sunspot model is adopted as shown in Figure 2 of Parker (1979), in which the field is divided into flux tubes some distance below the visible surface and the presumed convective downdraft helps to hold the separate flux tubes together in a tight cluster that constitutes the sunspot. These tubes are supposed to be formed at the base of the convection zone (CZ) from the global toroidal component of the solar magnetic field (Parker, 1993). McClymont and Jiao (1997) explained that mechanical forces can sustain torques in flux tubes that are not perfectly vertical and axisymmetric. However, for simplicity we assume that if no twist exists in flux tubes in the sub-photospheric plasma, they will be vertical and axisymmetric.

If the flux tubes are not twisted, they are perpendicular to the photosphere and to a certain "bottom" of the sunspot. Here, the bottom may or may not be the CZ base. It is such a surface above which the axes of the flux tubes are not deformed. In other words, below the photosphere the magnetic field vector can be expressed as $\boldsymbol{B}_i = B_{i0}\boldsymbol{e}_z$, where i refers to a certain flux tube marked by i.

We first carry out the integration over the sunspot surface below the photosphere. Over the lateral surface of the sunspot, it is obtained as

$$\boldsymbol{F}^{\mathrm{lat}} = \sum_i \int_{s_i} -\left(p_i + \frac{1}{2\mu_0}B_{i0}^2\right)\boldsymbol{n}_i\,\mathrm{d}s_i, \tag{2}$$

where $\boldsymbol{n}_i$ is the normal unit vector of the lateral surface $\mathrm{d}s_i$. Due to the isotropic property of gas and magnetic pressures, this term is equal to zero at the same depth. Over the bottom surface of the sunspot, the integration is obtained as

$$\boldsymbol{F}^{\mathrm{bot}} = \sum_i \int_{s_i} \left(p_i - \frac{1}{2\mu_0}B_{i0}^2\right)\boldsymbol{e}_z\,\mathrm{d}s_i. \tag{3}$$

Over the top surface of the flux at the photosphere, the magnetic field vector is $\boldsymbol{B} = B_x\boldsymbol{e}_x + B_y\boldsymbol{e}_y + B_z\boldsymbol{e}_z$ and the integration takes the form

$$\boldsymbol{F}^{\mathrm{top}} = \int \left\{\frac{1}{\mu_0}(B_z B_x \boldsymbol{e}_x + B_z B_y \boldsymbol{e}_y) + \left[\frac{1}{2\mu_0}\left(B_z^2 - B_x^2 - B_y^2\right) - p\right]\boldsymbol{e}_z\right\}\mathrm{d}x\,\mathrm{d}y. \tag{4}$$

Thus, three components of the LF are given in Cartesian coordinates:

$$F_x = \frac{1}{\mu_0}\int_{z=0} B_z B_x\,\mathrm{d}x\,\mathrm{d}y, \tag{5}$$

$$F_y = \frac{1}{\mu_0}\int_{z=0} B_z B_y\,\mathrm{d}x\,\mathrm{d}y, \tag{6}$$

$$F_z = \frac{1}{2\mu_0}\int_{z=0}\left(B_z^2 - B_x^2 - B_y^2\right)\mathrm{d}x\,\mathrm{d}y. \tag{7}$$

Here, the integrands are three components of the magnetic stress vector. At the horizontal direction, from Equations (1)–(4), there are the LF components $F_{\mathrm{m}x}$ and $F_{\mathrm{m}y}$ acting on the flux tubes below the photosphere. However, we do not know where the mass center of flux tube is located below the photosphere. It should move upwards as the sunspot emerges with time.

2.2. Magnetic Torques in Twisted Flux Tubes

What can we say about the LF integration for the twisted flux tubes of a rotating sunspot? In this case, there might be a magnetic torque leading to twist in the horizontal field. The magnetic vector is assumed to be $\boldsymbol{B} = B_\phi \boldsymbol{e}_\phi + B_z \boldsymbol{e}_z$ in cylindrical coordinates. The integration of the first term on the right-hand side of Equation (1) is still equal to zero over the lateral surface and the integration at the top surface of the flux tubes under the photosphere is the same as Equation (4). The integration at the bottom surface is also similar to Equation (4) except with a minus sign since the normal direction of the bottom surface being contrary to that of the sunspot surface at the photosphere. Thus, the magnetic torque on a section of the tube is (Longcope and Klapper, 1997)

$$\boldsymbol{T}_{\mathrm{m}} = \frac{1}{\mu_0}\int \left[\boldsymbol{r} \times (B_\phi \boldsymbol{e}_\phi)\right](\boldsymbol{B}\cdot\boldsymbol{n})\,\mathrm{d}S, \tag{8}$$

where $\boldsymbol{r}$ is the distance of magnetic torque relative to the center of mass.

On the other hand, how about the forces acting on the sunspot above the photosphere? Molodenskii (1974) and Low (1985) pointed out that for an isolated magnetic structure located in the infinite half-space above the plane $z = 0$, the LF in the volume $z > 0$ is just the Maxwell stress integrated over the plane $z = 0$, provided that the field falls off fast enough as z goes to infinity. In Cartesian coordinates, F_x, F_y, and F_z are simply computed from

$$F_x = -\frac{1}{\mu_0}\int_{z=0} B_z B_x\,\mathrm{d}x\,\mathrm{d}y, \tag{9}$$

$$F_y = -\frac{1}{\mu_0}\int_{z=0} B_z B_y\,\mathrm{d}x\,\mathrm{d}y, \tag{10}$$

$$F_z = -\frac{1}{2\mu_0}\int_{z=0}\left(B_z^2 - B_x^2 - B_y^2\right)\mathrm{d}x\,\mathrm{d}y, \tag{11}$$

and

$$F_{\mathrm{p}} = \frac{1}{2\mu_0}\int_{z=0}\left(B_z^2 + B_x^2 + B_y^2\right)\mathrm{d}x\,\mathrm{d}y, \tag{12}$$

where F_{p} is the integrated magnetic pressure force. According to Low (1985) necessary conditions for the magnetic field to be force-free are that $|F_x| \ll F_{\mathrm{p}}$, $|F_y| \ll F_{\mathrm{p}}$, and $|F_z| \ll F_{\mathrm{p}}$. Metcalf *et al.* (1995) was the first to use the above formulae to study whether photospheric magnetic fields are force-free or not and they concluded that the magnetic field is not force-free in the lower photosphere, but becomes force-free roughly 400 km above the photosphere. However, Moon *et al.* (2002) suggest that the photospheric magnetic fields are not as far from a force-free equilibrium as previously thought. Recently, Georgoulis and LaBonte

(2004) calculated the vertical LF and a corresponding lower limit of the cross-field electric current density and gave a clear conclusion that the photospheric active region magnetic fields are not force-free, contrary to conjectures of some recent studies.

From that, Equation (8) can be used to formulate the magnetic torque on the photosphere, which is a result of only a fraction of the volume current carried by the twisted flux tube passing into the corona along field lines and an equal return current passing along the photosphere (Longcope and Welsch, 2000). Therefore, transport of the flux tube's twist from the photosphere to the corona will be suppressed for a time $\tau_A = d_0/v_A$, where d_0 and v_A are the typical coronal length scale and the Alfvén velocity, respectively. The torque from this surface current can initiate a plasma rotation, which, along with the twist suppression, forms a torsional wave propagating downward from the photosphere (Longcope and Welsch, 2000).

Magnetic neutral lines (MNLs) are the special loci on the solar surface, at which the vertical component of the magnetic fields vanishes. The forces from Equations (5) – (7) are negligible compared to hydrodynamic forces below the photosphere. Therefore, in theory to obtain the LF acting on a closed space containing the MNLs, we do not need to consider the contributions from the half-space under the photosphere. This indicates that in the observations we might use Equations (9) – (11) to calculate the LFs near the MNLs. However, when using them, we also need to make a similar assumption to Low (1985) that the horizontal magnetic field falls off fast enough as z goes to infinity. Manchester (2001) simulated the emergence of a flux rope and found that its two sides move in opposite directions as the flux rope expands. The motions of the flux rope are driven by the LF. Therefore, the LF acting on the MNL region can provide both a driving force and a driving torque for horizontal motion and rotation of a sunspot, respectively.

2.3. Opposite Vortical Flows and Magnetic Torques

Zhao and Kosovichev (2003) applied methods of the time-distance helioseismology to study the sub-photospheric structures and dynamics of an unusually fast-rotating sunspot observed by the Michelson Doppler Imager on board SOHO in August 2000. The subsurface sound speed structures and velocity fields are obtained for the sunspot region at different depths from 0 to 12 Mm. Seen from above, in the depth range of 0 – 3(5) Mm, there is a downward, converging flow with a counterclockwise (CCW) rotating direction; while in the depth range of 9 – 12 Mm, there is an upward, divergent flow with a clockwise (CW) rotating direction. They used a hurricane on the Earth to make an analogy. Thus, the opposite vortical flows may be caused by Coriolis force. However, the question is why vortical flows are not observed in most sunspots.

Based on the simulations of Longcope and Welsch (2000) and Manchester (2001), we try to explain this issue in terms of the interaction of magnetic forces and sub-photospheric plasma to make a qualitative analysis. On the whole, the basic idea is to make a magnitude comparison between the magnetic force $\boldsymbol{F}_m$ and the nonmagnetic force $\boldsymbol{F}_{nm}$. When $\boldsymbol{F}_{nm} > \boldsymbol{F}_m$, magnetic energy will be built up, while when $\boldsymbol{F}_{nm} < \boldsymbol{F}_m$, the stored magnetic energy will be released.

First, we assume that the large-scale sub-photospheric vortical flow is the most plausible driving factor to twist the magnetic flux tubes. The above two observed, opposite vortical flows below the photosphere work together to twist the flux tube (named Assumption 1). Second, we assume that they are generated by the relaxation of the already twisted flux tube (named Assumption 2). For simplicity, the expansion of the flux tube is neglected. In the first case, there are two opposite nonmagnetic torques (from two observed vortical flows) acting

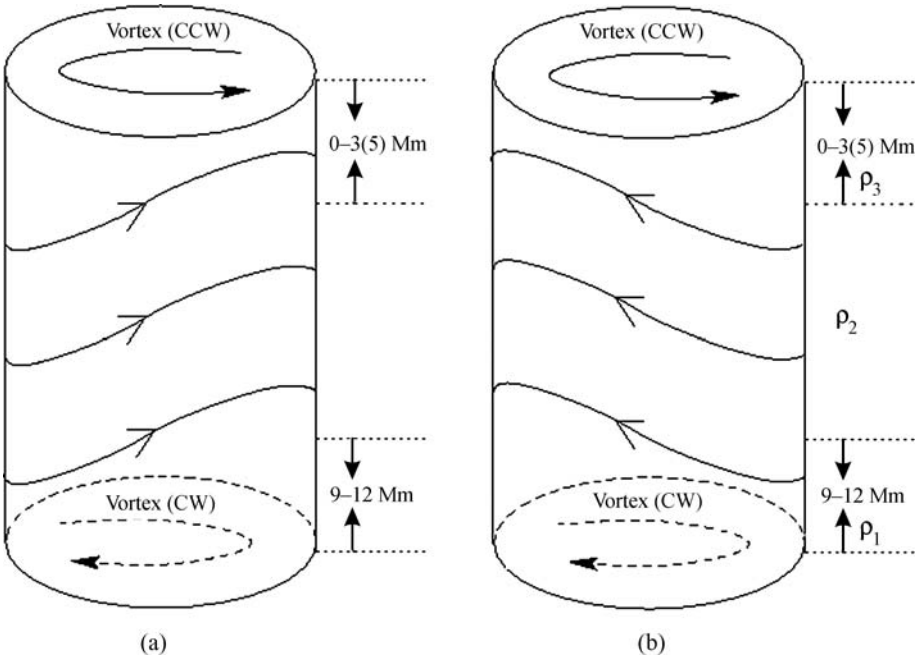

Figure 1 The relationship of a flux tube with two opposite vortical flows below the photosphere in the depth range of 0 – 12 Mm. (a) The flux tube is being twisted by two flows. (b) The twisted flux tube creates two flows.

on a part of the flux tube under the photosphere. By checking the vector magnetograms on 9 August 2000, we find that the longitudinal field of active region NOAA 9114 is of positive polarity and the transverse field exhibits a CW trend. According to the model of Longcope and Welsch (2000), a uniformly twisted flux tube would remain uniformly twisted, and twisting motions will arise in a flux tube with twist variations along its length, to make twist uniform. Therefore, we believe that the flux tube of NOAA 9114 under the photosphere is CW twisted as well.

Figure 1(a) shows a flux tube with CCW twist introduced by two opposite nonmagnetic torques, $T1_{\rm nm}$ and $T3_{\rm nm}$. $T1_{\rm nm}$ is coming from a CW vortical flow located in the depth range of 9 – 12 Mm and $T3_{\rm nm}$ from a CCW vortical flow in the depth range of 0 – 3(5) Mm, which act together on the flux tube. If so, two horizontal magnetic forces, $F1_{\rm m}$ (CCW) and $F3_{\rm m}$ (CW) acting on the two vortical flows, will be created to counteract the nonmagnetic forces $F1_{\rm nm}$ and $F3_{\rm nm}$, respectively. On the other hand, because the twisted flux tube in the depth range of 0 – 12 Mm is taken as one whole, the normal unit vectors at its bottom and top surfaces are $-\boldsymbol{e}_z$ and $\boldsymbol{e}_z$, respectively. Thus, according to Equation (8), we find the handedness of $F1_{\rm m}$ and $F3_{\rm m}$ are really CCW and CW, respectively.

However, it may be not possible that two sub-photospheric vortical flows are the driving factors of twist. First, when two opposite nonmagnetic torques act together on a flux tube, it must contract as the twist increases. Therefore, we expect that the contraction would lead to upward flows at the upper region (0 – 3(5) Mm), and downward flows at the lower region (9 – 12 Mm), as plasma is squeezed out of the shrinking flux tube. But according to the observations of Zhao and Kosovichev (2003), the former flow is downward and the latter is upward. Second, near the photosphere (0 – 12 Mm), the nonmagnetic force may be

less than or equal to the magnetic force. The vortical flows may not be able to drive the flux tube to twist effectively. Last, maybe it is very rare that two vortical flows could align vertically and work together to twist a flux tube. For these reasons, we assume that the opposite vortical flows could be driven by the restoring forces (LFs) coming from the twisted flux tube in the depth range of 0 – 12 Mm (even though the plasma is high β). Figure 1(b) shows this physical process and in this case, the twist of the flux tube should be CW.

At first, in the deeper zone under the photosphere, to maintain such a twist, there must be two horizontal nonmagnetic forces of $F1_{\rm nm}$ (CCW) and $F3_{\rm nm}$ (CW) acting on a section of the flux tube. The former is located at the bottom and the latter is on the top of it. Both of them can be calculated with Equation (8). At the same time, there exist two magnetic forces of $F1_{\rm m}$ (CW) and $F3_{\rm m}$ (CCW) acting on the surrounding plasma of the flux tube. As it emerges upwards, $F1_{\rm nm}$ (CCW) and $F3_{\rm nm}$ (CW) may become weaker and weaker with the decrease of plasma density. In the depth range, *e.g.*, 0 – 12 Mm, the magnetic forces may be greater than the nonmagnetic forces so that they are able to drive the plasma to rotate oppositely in the two ends. This means that there are two opposite vortical flows created around the flux tube. A CW flow on the bottom will decrease the tube's CW twist, and a CCW flow on the top will also decrease the tube's CW twist. As the tube becomes less twisted, the magnetic pressure in the tube will decrease, which will cause gas to flow into the tube from above and below to establish pressure equilibrium. This is actually what the observations of Zhao and Kosovichev (2003) show: a downflow into the tube from above, and an upflow into the tube from below. This interpretation is consistent with the data.

Moreover, the opposite vortical flows turn to initiate a CCW and a CW Alfvén wave passing upwards and downwards along the flux tube, respectively. They both decrease the CW twist of the flux tube. We think this may be another reason for the suppression of the twist increase in the corona distinct from the flux tube expansion at the stage of emergence (Longcope and Welsch, 2000). Our model seems to support a previous finding by Leka *et al.* (1996) that currents are generated below the photosphere prior to flux emergence instead of vortical motions in the photosphere.

Furthermore, we divide the zone in the depth range of 0 – 12 Mm into three regions in terms of plasma density, R3: 0 – 3(5) Mm, R2: 3(5) – 9 Mm and R1: 9 – 12 Mm. The respective densities are $\rho 3 < \rho 2 < \rho 1$. R2 is a region of transition, where the flow velocity is expected to be zero. Actually, there was no vortical flow reported by Zhao and Kosovichev (2003) either. The kinetic energy in R1 and R3 should satisfy the relationship

$$\int_{\rm R1} \frac{1}{2}\rho_1 V_1^2 \,{\rm d}^3 r + \int_{\rm R3} \frac{1}{2}\rho_3 V_3^2 \,{\rm d}^3 r \leq \int_{\rm R1,3} \frac{1}{2\mu_0} B^2 \,{\rm d}^3 r. \tag{13}$$

2.4. Nonpotential Magnetic Stress

The dimension of the integrands in Equations (5) – (7) is the force per unit area or the energy per unit volume. In this subsection, we continue to analyze the LF in terms of the energy. We define such a vector, the nonpotential magnetic stress (NPMS) as follows:

$$\tau_x = \frac{1}{\mu_0} B_z B_x - \tau_x^{\rm p}, \tag{14}$$

$$\tau_y = \frac{1}{\mu_0} B_z B_y - \tau_y^{\rm p}, \tag{15}$$

$$\tau_z = \frac{1}{2\mu_0}\left(B_z^2 - B_x^2 - B_y^2\right) - \tau_z^{\mathrm{p}}, \tag{16}$$

where τ_x^{p}, τ_y^{p} and τ_z^{p} are the corresponding potential quantities extrapolated from the observed longitudinal (not normal) magnetic field. To define τ_x, τ_y and τ_z, we use the integrands in Equations (5) – (7) instead of those in Equations (9) – (11) because we want to study the evolution of magnetic energy from sub-photosphere to corona. In the next section, we will apply the obtained formulae to calculate the LF acting on a horizontally moving rotating sunspot on 11 December 2006.

3. Instruments and Data

The main data used in this work include G-band filtergrams and the high-resolution vector magnetic fields taken by the Solar Optical Telescope (SOT) onboard *Hinode*, and low-cadence vector magnetic fields taken by the Solar Magnetism and Activity Telescope (SMAT) installed at Huairou Solar Observing Station of Beijing. In addition, we use SOHO/MDI (Scherrer *et al.*, 1995) full-disk magnetograms to study the motion of the main sunspot in the NOAA AR 10930.

3.1. *Hinode*/SOT and Data

The SOT is optimized for measurement of the vector magnetic field and associated dynamics in the solar photosphere and chromosphere (Kosugi *et al.*, 2007; Ichimoto *et al.*, 2008; Shimizu, 2004). It can obtain a continuous, seeing-free series of diffraction-limited images (0.2 – 0.3 arcsec) in the 388 – 668 nm range. The SOT consists of the Optical Telescope Assembly (OTA) which is an aplanatic Gregorian telescope with the aperture size of 500 mm, and the Focal Plane Package (FPP) which produces scientific data on two CCD cameras with filter and spectral instruments. In filter observations, a $4k \times 2k$ CCD camera is shared by the broadband filter imager (BFI) and the narrow-band filter imager (NFI). That the BFI produces photometric images at 430 – 431 nm is the CH G-band observation. SOT or BFI will allow accurate measurements of magnetic elements and horizontal flows in the photosphere at the highest possible spatial resolution (0.0541 arcsec pixel^{-1} sampling) and at rapid cadence (< 10 s typical) over a full field of view of 218×109 arcsec. Spectral observations provide detailed Stokes profiles of the magnetically sensitive Fe I nm line that allow for the sophisticated analysis to determine all the magnetic vector components.

3.2. Huairou/SMAT and Data

The SMAT was developed to study large-scale magnetic activity on the Sun (Zhang *et al.*, 2007). It consists of two instruments: a 10 cm telescope performing full-disk vector magnetic field observations, and a 20 cm telescope performing full-disk Hα observations. The core element of the magnetograph is a birefringent filter with a 0.125 Å bandpass. The filter is installed in a telecentric optical beam to overcome the variation of the pass-band of the filter in different positions of the image plane. The temporal and spatial resolution are about 5 min and 5 arcsec, respectively, if the magnetogram is taken with the sum of 1024 individual frames. The magnetograph uses the spectral line Fe I $\lambda = 5324.19$, with a total half-width of 0.334 Å (a Landé factor of $g = 1.5$). An introduction to the observation and calibration of the vector magnetograms can be found in Su and Zhang (2007).

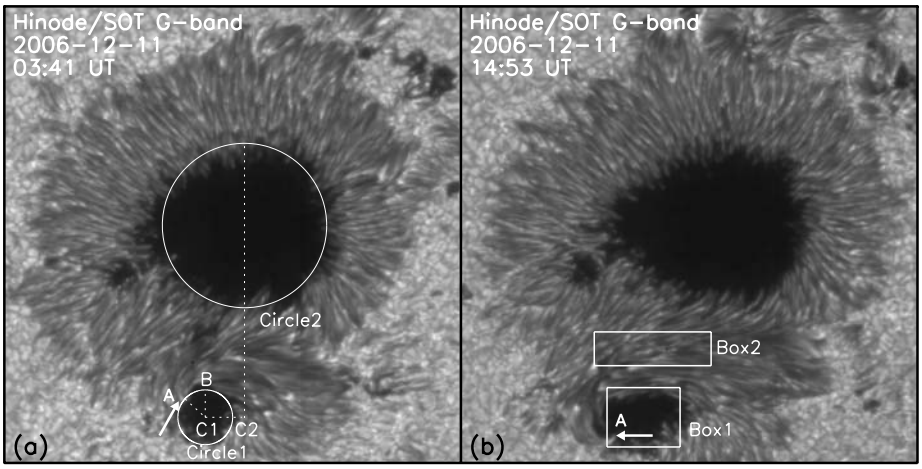

Figure 2 Two *Hinode*/SOT images taken on 11 December 2006 at (a) 03:41 UT and (b) 14:53 UT. For an explanation of the circles and boxes shown here see the text. Sunspot S1 (the smaller one) is moving to the left (eastward) relative to sunspot S2 (the larger one). At the same time, S1 rotates counterclockwise. The field of view is 72 × 72 arcsec. North is up and west is to the right.

4. Observations and Results

4.1. Uniform Motions of Sunspot

During the period of 6 – 14 December 2006, in the declining phase of the solar cycle, AR 10930 produced four X-flares. The multiple flaring appears to be associated with a small emerging and rotating sunspot (S1) around a larger stable sunspot (S2). In this paper, we examine the uniform motions of the sunspot S1 on 11 December prior to the course of the major event of 13 December with the emphasis on the LF acting on this sunspot. Note that AR 10930 was located near the disk center on 11 December 2006.

Figure 2 presents the *Hinode*/SOT G-band observations for the active region at 03:41 UT (left) and 14:53 UT (right) on 11 December 2006. In the period of 00:00 UT – 15:00 UT, the sunspot S1 grew gradually and rotated CCW. At the same time, it also moved horizontally to the left. We have noticed that several dark threads connected the opposite polarity pair of sunspots S1 and S2. A bright feature at the edge of sunspot S1 is marked as "A" indicated by a white arrow. We monitor the position variation of the feature "A" and the horizontal displacement of the sunspot S1 relative to sunspot S2 to study the dynamic evolution of sunspot S1.

The method is to find the centroid and the radius of each sunspot umbra. First, the umbra centroid is calculated as the brightness-weighted center of the umbra region. Then, we can obtain the derivatives of the brightness variations along the two lines across the centroid. The radius of the umbra is thus defined as the average value of the distances of the four inflexions relative to the centroid. Two circles obtained by the above method are plotted on the left panel of Figure 2. C1 and C2 are the x centroid positions of the two circles and "B" is the intersection of the line running across the centroids of the sunspot S1 and the circle 1.

By checking the SOHO/MDI full-disk magnetograms on 11 December, we find that the field strength-weighted center of sunspot S2 changed not more than 0.4 arcsec on that day. Therefore, we think the major sunspot S2 was very stable and the relative displacement

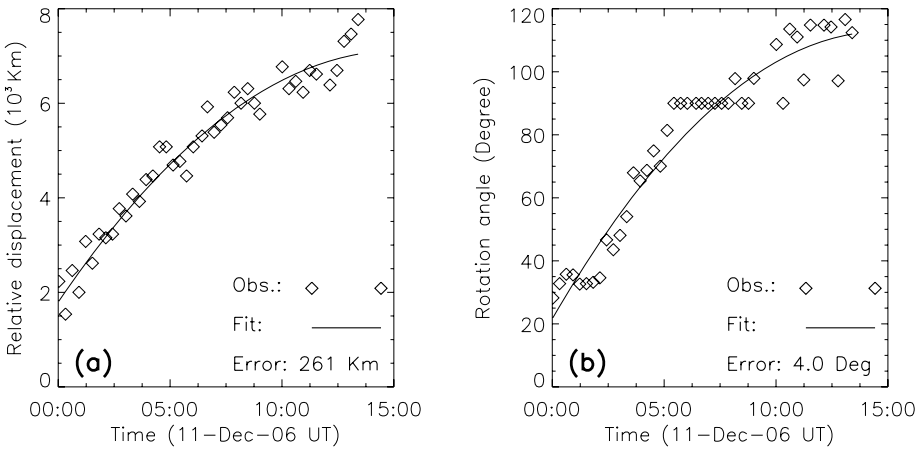

Figure 3 (a) The displacement L_{c1-c2} *vs.* time; (b) the angle $\angle AC1B$ *vs.* time.

L_{c1-c2} between C1 and C2 can be used to study the horizontal motion of the sunspot S1 in the x-axis direction. Figure 3 shows the evolution of L_{c1-c2} and the rotation angle of $\angle AC1B$ with time in Cartesian coordinates, the x-axis and y-axis point to the right and upward, respectively. Their measurement errors are also given on the plot. A second order polynomial was fitted to the data. The acceleration of the horizontal motion is -2.8×10^{-9} m s^{-2} and the angular acceleration of the rotation is -5.1×10^{-8} deg s^{-2} (CW). Similarly, Brown *et al.* (2003) observed rotating sunspots accelerating from rest to speeds of 1 deg hr^{-1} over 20 hours, or about 4×10^{-9} deg s^{-2}. The motions slowed down in the period of about 15 hours, but the accelerations were very small in magnitude. Therefore, we think the sunspot S1 exhibited uniform motions. Were there counter-balancing forces and torques acting on the moving sunspot and if so, what was their origin?

4.2. Observed Magnetic Forces

In Section 2.3, we adopt Assumption 2 that the relaxation of a CW twisted flux tube is to drive two opposite vortical flows in the depth range of 9 – 12 Mm. Therefore, a CCW Alfvén wave will be initiated passing upwards and a CW Alfvén wave passing downwards along the flux tube. However, the downward Alfvén speed falls dramatically with increasing depth below the photosphere due to the increase of plasma density. Thus, magnetic evolution at the photosphere is decoupled from magnetic fields in the deep interior. On the other hand, the upward Alfvén wave will bring the information of the CCW magnetic torque across the photosphere. It indicates that the calculated magnetic stress at the photosphere may reflect the magnetic tension below the photosphere. According to Equation (8), the magnetic tension, in the depth range of 9 – 12 Mm, can be calculated with Equations (9) – (11). So the magnetic stress at the photosphere can be calculated as well.

Figure 4 shows the SP/SOT vector magnetogram (left) of sunspot S1 marked by Box 1 in Figure 2 and the longitudinal and transverse components of magnetic stress (right) calculated with Equations (9) – (11). This vector magnetogram is taken from the average of three sets of SP/SOT vector magnetograms observed starting at 03:10 UT, 08:00 UT and 11:10 UT. It should be noted that we do not correct for the differential rotation of the Sun, which may not be significant when the active region is close to the disk center. Here the

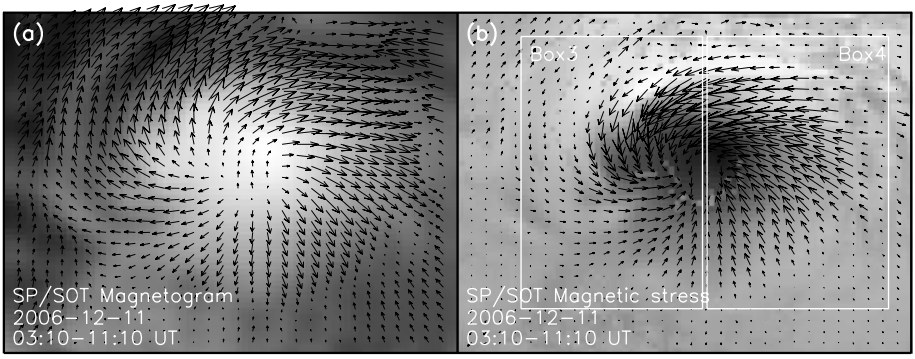

Figure 4 (a) Averaged SOT/SP vector magnetogram taken between 03:10 UT – 11:10 UT. The longitudinal field strength is scaled between ±3000 G and the largest value of transverse field 2513 G; (b) the magnetic stress in longitudinal and transverse directions. Its longitudinal component is scaled between $\pm 3.8 \times 10^8$ N m^{-2} and its largest value of transverse component 4.3×10^8 N m^{-2}. The field of view is marked by Box 1 in Figure 2.

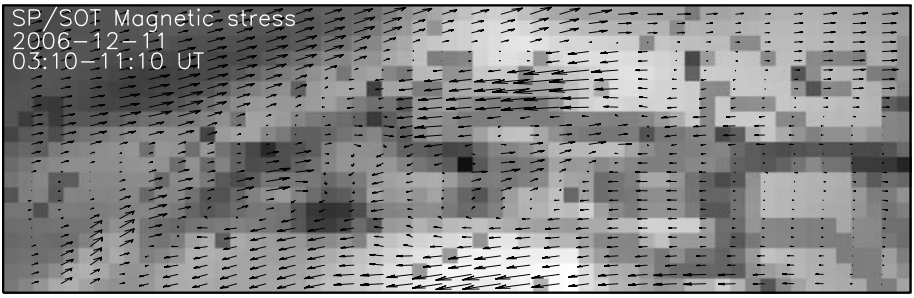

Figure 5 A map of the magnetic stress around the magnetic neutral line. The scale is the same as that of Figure 4(b). The field of view is shown in Figure 2 marked by Box 2.

integral of the longitudinal magnetic stress in the umbra region of the sunspot should be negative, which is consistent with the result of Moon *et al.* (2002).

The LF integral in Box 3 of Figure 4b is $F_{y3} = -3.28 \times 10^{21}$ N and that in Box 4 is $F_{y4} = 2.73 \times 10^{21}$ N. The umbra radius of the sunspot S1 is about 4 Mm (the time-averaged value). Therefore, there is a upward, vertical magnetic torque, about 5.8×10^{27} N m, acting on sunspot S1. The torque might play a role in driving the sunspot to rotate. Now, how about the magnetic stress in the region around the MNL? Figure 5 shows the magnetic stress obtained with Equations (9) – (11) in a MNL region marked by the white Box 2 in Figure 2. The rules of selecting the region are that (1) the positive and negative integrals of the LF should be approximately equal, and (2) the LOS component of the magnetic fields is as small as possible. Therefore, we choose such a region in which the average LOS field strength decreases to about one tenth of the maximum field strength of the umbra region of sunspot S1.

The positive integral of the LF in x-axis direction is $F_{x+} = 1.38 \times 10^{21}$ N and the negative integral is $F_{x-} = -1.23 \times 10^{21}$ N. The negative force is consistent with the rotation direction of sunspot S1, and thus it should also drive the sunspot to rotate. If we assume that the CCW rotating length-scale of sunspot S1 is 5 Mm thick, an estimation of the mass of sunspot S1

yields about $M_{S1} = 7.5 \times 10^{22}$ kg. We adopt a value of 3.0×10^2 kg m^{-3} for the density of the sunspot, which is an average density value at the base of the CZ (Priest, 1984). If F_{x-} acts on it, an acceleration of 1.6×10^{-2} m s^{-2} will be created. The magnetic torque caused by F_{x-} is about 4.7×10^{27} N m, which is also vertically upward. Thus, including the above torque of 5.8×10^{27} N m, we obtain for the total upward torque about 1.1×10^{28} N m. The moment of inertia of this segment of tube is $I = \frac{1}{2}Mr^2$. With the torque of 1.1×10^{28} N m, mass of 7.5×10^{22} kg, and radius of 4 Mm, we get an angular acceleration of 1.8×10^{-8} rad s^{-2}, or about 1.0×10^{-6} deg s^{-2} (CCW).

It seems that the calculated and the observed angular accelerations are different in both magnitude and direction. The reason is that in the above calculations, we do not include the magnetic torque contribution coming from the tube's bottom surface at the depth of 5 Mm. According to Equation (8), the magnetic torque at this bottom surface is equal to the difference between the observed torque at the top surface and the product of the observed angular acceleration with the moment of inertia $T_b = -T_t^{obs} + I\dot{\Omega}^{obs}$. Thus, the bottom surface torque is -2.0×10^{28} N m.

This magnetic torque could be used to constrain the field line twist on the bottom surface of the flux tube, of which two magnetic field components satisfying the constraint $B_\phi = qrB_z$ are assumed, where q is the tube's pitch on the bottom. An evaluation of the magnetic torque on the bottom at 5 Mm is formulated as $T_b = \frac{\pi}{2\mu_0} q_b r_b^4 B_{zb}^2$, where all arguments are average values, subscript z presents the normal magnetic field component, and subscript b presents the bottom surface. Since the total normal flux on the bottom equals the total normal flux on the top, the magnetic torque could also be given as $T_b = \frac{\pi}{2\mu_0} q_b r_t^4 B_{zt}^2$ in terms of the normal magnetic field component of B_{zt} on the top surface. In Figure 4(a), the mean value of the longitudinal field component is 1060 G. If $r_t = 4$ Mm, we then obtain the value of q_b, 6.25×10^{-3} m^{-1}.

4.3. The Observed Nonpotential Magnetic Stress

Nonpotentiality of the magnetic structure in an active region is an important indicator of stored energy which is released in flares. The most notable indicator of non-potentiality is a δ sunspot. Other viable proxies are magnetic shear and magnetic gradient of LOS magnetic field and so on. Wang *et al.* (2006) found an apparent correlation between magnetic shear and magnetic gradient at a level of about 90%. Furthermore, they found that the magnetic gradient could be a better proxy than the shear for predicting where a major flare might occur. In this subsection, we use the nonpotential magnetic stress (NPMS), $\boldsymbol{\tau}$ (τ_x, τ_y, τ_z), as a flare proxy and study its evolution in the X3.4 flare event starting at 02:14 UT on 13 December 2006 in AR 10930.

The vector magnetograms of the AR 10930 were taken from the Huairou full-disk SMAT magnetograph system at the wavelength offset $+0.08$ Å of the line Fe I $\lambda = 5324.19$. The potential method is used to resolve the 180-degree ambiguity in transverse magnetic field. Li (2002) simulated the projection effects, and found that they would add about 10% to the uncertainty at the largest off-center position of the observed regions. The AR 10930 was not far away from the disk center at about S06W21 at 00:00 UT of 13 December. In Figure 6, we show two vector magnetograms before and after the observed flare. The first one is an average of four vector magnetograms taken at 00:46 UT, 00:54 UT, 01:08 UT and 01:31 UT, and the other is of two taken at 05:35 UT and 06:30 UT.

The evolution of the vector $\boldsymbol{\tau}$ from 00:46 UT to 05:32 UT is shown in Figure 7. For the SMAT data, there is a big time gap between 03:03 UT and 05:32. So the SP/SOT data at 04:30 UT were adopted to supplement those taken by the SMAT. In order to match the

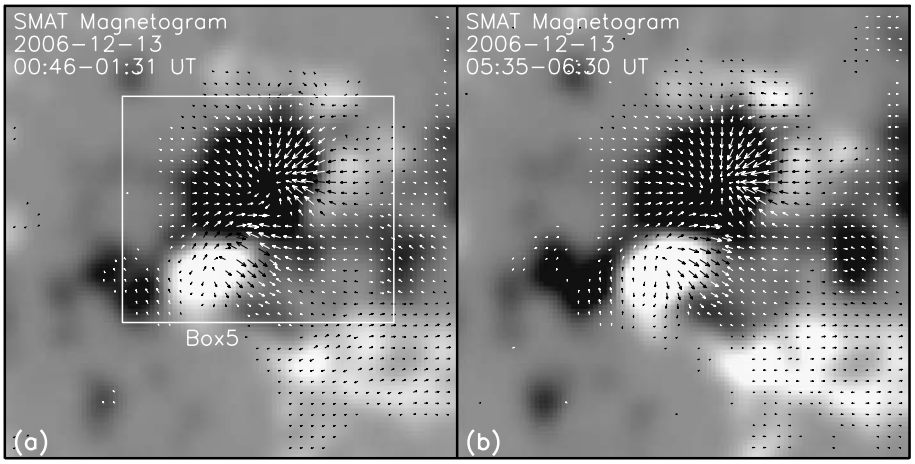

Figure 6 The SMAT vector magnetograms (a) before and (b) after a major X3.4 flare on 13 December 2006. The flare started at 02:14 UT and peaked at 02:40 UT. The field of view is 200 × 200 arcsec.

spatial resolution of 5 arcsec of the SMAT, we carry out a smoothing of the SP/SOT data over 15 × 15 pixels. By comparing the SMAT longitudinal field at 03:03 UT with that of the SP/SOT at 04:30 UT, the SMAT longitudinal fields have been multiplied by a factor of 5. Furthermore, a factor of 3.9 has been applied to the SMAT transverse fields in comparison with the corresponding potential quantities extrapolated from the above corrected longitudinal fields. There is a flaw in the above comparisons, which is that we do not take into account the filling factor when dealing with SMAT and SP/SOT data.

The LOS component τ_z is presented by the gray-scale patches and the transverse component, τ_t ($\sqrt{\tau_x^2 + \tau_y^2}$) by the arrows. The field of view is marked with the white Box 5 in Figure 6. The increase of τ_z along the MNL was obvious from 00:46 UT to 03:02 UT. In our figure, it reached the maximum on the panel of 03:02 UT at the end of the flare (02:57 UT). There are two features for the τ_t in both sunspots and around the neutral line. First, the arrows point to the line with an angle, then become flat along the line, further point off the line with an angle (as if they were reflected back). Second, the mean angle between the arrows pointing to and off the neutral line became large when the time approached the onset of the flare, and they were nearly 180° at 03:02 UT (at the end of the flare). Moreover, at 03:02 UT, in the umbra of sunspot S2, the value of τ_t was very small.

To quantitatively show the evolution of the magnetic stress, we make the integrations of τ_z and τ_t in AR 10930 and list them in Table 1. The quantities of E_{+z}^{fov} and E_z^{B6} are the integrals of the positive τ_z in the whole field of view and in Box 6 (around the neutral line), respectively. It is obvious that they successively increased prior to and during the flare and decreased to minima after the flare at 05:32 UT in our data. E_z^{B6} in the second column accounted for about 50% of E_{+z}^{fov} in the fourth column. This indicates that the region around the MNL is the major site of magnetic energy release for the flare. The last column is the quantity E_t^{fov}, the integral of τ_t in the whole field of view. E_t^{fov} is an order of magnitude larger than E_{+z}^{fov} or E_z^{B6}. This fact combined with the features of τ_t introduced above may give a hint that the transverse component of the magnetic stress gets transported to the magnetic neutral line and then part of it changes into the line of sight component of the stress. That is

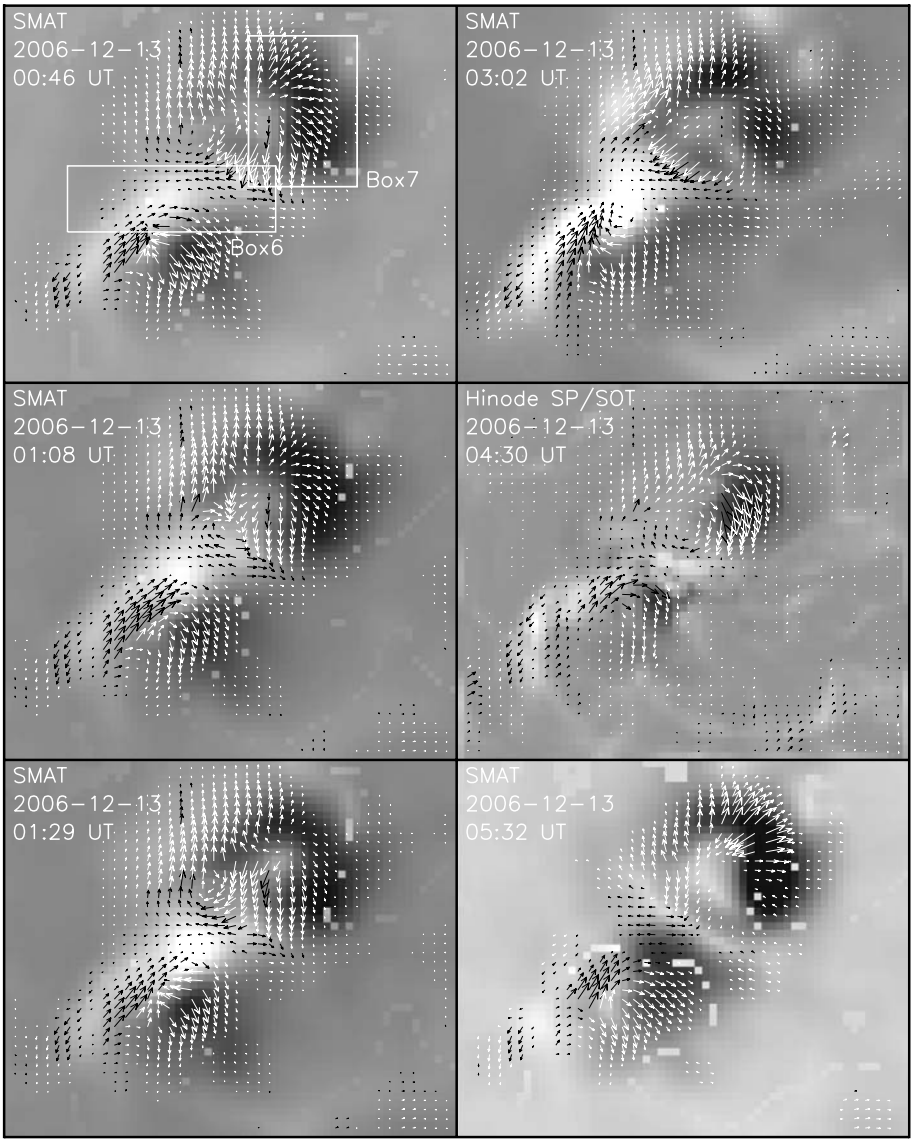

Figure 7 Time sequence of the vector τ from 00:46 UT to 05:32 UT. Its LOS component τ_z is scaled between $\pm 3.8 \times 10^8$ erg m^{-3} and its maximum transverse component τ_t is 4.3×10^8 erg m^{-3}. The black and white vectors coincide with regions of positive and negative τ_z. The field of view is 120×100 arcsec.

the magnetic energy in the horizontal direction gets transported to the neutral line, and then partly changes into the energy in line of sight direction for the flare.

However, magnetic energy is transported by the Poynting flux, and "transport" implies the motion of magnetic fields, which can be determined from magnetic tracking (Liu and Zhang, 2006). It is unclear how NPMS relates to energy transport inferred from the Poynting flux estimated by tracking. Therefore, we need other data, such as magnetic tracking, to

Table 1 The integral of the nonpotential magnetic stress.

Integral of $\tau_{t,z}$ (10^{23} erg m^{-3})					
Time (UT)	E_{+z}^{fov}	E_{-z}^{fov}	E_{z}^{B6}	E_{z}^{B7}	E_{t}^{fov}
00:46	0.71	−3.38	0.42	−1.51	6.92
01:08	1.67	−3.27	0.85	−1.65	9.01
01:29	2.06	−2.92	1.06	−1.43	11.0
03:03	3.26	−2.09	1.12	−1.16	11.3
04:30	0.74	−0.50	0.16	−0.36	3.25
05:32	0.10	−4.78	0.02	−1.92	3.39

In the Table 1, E_{+z}^{fov} and E_{-z}^{fov} are the integrals of the positive and negative τ_z, and E_{t}^{fov} is the integral of τ_t in the whole field of view. E_{z}^{B6} and E_{z}^{B7} are the integrals of τ_z in the Boxes 6 and 7 shown in Figure 7.

support the above magnetic energy transport assumption. In addition, it is very interesting that the absolute values of E_{-z}^{fov} and E_{z}^{B7} were decreasing from 00:46 UT to 04:30 UT and then increasing to the maximums at 05:32 UT in our data. In future work, it is worthwhile to analyze in more detail what the relationship is between E_{+z} and E_{-z} in the process of the flare.

5. Discussion and Conclusions

In our view, the magnetic tension should be a restoring force for the rotation of a sunspot produced by a perturbing force from other sources, for instance, the large-scale vortical flows under the photosphere. As a restoring force, when it is greater than the other forces, the magnetic tension will bring the sunspot system back toward the initial equilibrium of lower energy status. All our thoughts in the current work are based on the above idea.

In this paper, we present a qualitative analysis of the interaction of sub-photospheric magnetic force and plasma. To study the sub-photospheric vortical flows around a fast rotating sunspot observed by Zhao and Kosovichev (2003), we make two assumptions to explain this phenomenon: the twist of flux tube is (1) caused by two flows; (2) driving two flows. For the first one, the flux tube will contract under the actions of two nonmagnetic torques, so we will only observe the upward flows in the depth range of 0 – 3(5) Mm and the downward flows in the depth range of 9 – 12 Mm below the photosphere. However, this is in contradiction with the observations of Zhao and Kosovichev (2003). Therefore, we prefer the second assumption that the relaxation of a twisted flux tube causes two vortical flows.

However, our simple analysis of a rotating sunspot is not sufficient to explain the abundant physical phenomena involved in it. Linton, Longcope, and Fisher (1996) argued that as a flux tube emerges, the critical twist necessary for the onset of the kink instability decreases. The twist of the rising tube, which stays constant, might then exceed this new (lower) critical twist. It indicates that the apex of flux loop could become kink unstable. This means that our analysis cannot exclude the possibility of the occurrence of kink instability as the flux tube rises across the photosphere. In our model, the upward counterclockwise torsional Alfvén wave will lead to a suppression of twist propagation from sub-photosphere to corona.

In the observations, our model is used to analyze another rotating sunspot in the active region NOAA 10930 on 11 December 2006. We assume that it is a common phenomena for the occurrence of two sub-photospheric opposite vortical flows around a rotating sunspot. We find that the sunspot exhibited a uniform horizontal motion eastward and a uniform counterclockwise rotation from 00:00 UT to 15:00 UT. It may be a result of the balance between the magnetic torques in two ends of a section of flux tube. We have determined that the magnitude of the total magnetic torque is about $10^{27} \sim 10^{28}$ N m in this active region.

To study the evolution of magnetic energy near the photosphere, we define a vector, the nonpotential magnetic stress (NPMS) as described in Equations (14) – (16). However, in the observations there is difficulty in determining this new vector. The quality of vector magnetic data greatly depends on the method of the resolution of the 180-degree ambiguity. Although the SMAT data appear satisfactory, further examination will be necessary to establish its quality.

By studying the evolution of NPMS, we find that: (1) the integral of its LOS component successively increases around the magnetic neutral line (MNL) prior to and during the flare and decreases to the minimum after the flare; (2) the integral of its transverse component exceeds the integral of its LOS component by one order of magnitude over the whole field of view; (3) the transverse component first points toward the MNL, and then along it, finally it points backward. It seems that the magnetic energy in the horizontal direction gets transported to the neutral line, and then partly changes into the energy in LOS direction for the flare. However, whether or not this is the case will be shown by the Poynting flux, which can be determined from tracking the displacements of magnetic field concentrations (Liu and Zhang, 2006). This will be the subject of our future work.

Acknowledgements We wish to address our sincere thanks to the referee for giving the paper substantial suggestions and comments. We thank Dr. Lidia van Driel-Gesztelyi and the language editor for helpful editorial work. This work is supported by the NSFC projects (nos. 10611120338, 10673016, 60673158, 10473016, and 10273002), National Basic Research Program of China under grant 2006CB806301, Important Directional Project of Chinese Academy of Sciences KLCX2-YW-T04, and the NAOC innovation project of 2007. *Hinode* is a Japanese mission developed and launched by ISAS/JAXA, with NAOJ as domestic partner and NASA and STFC(UK) as international partners. It is operated by these agencies in cooperation with ESA and the NSC (Norway). We are also grateful to all members of the SOHO MDI team for providing the wonderful data. SOHO is a project of international cooperation between ESA and NASA.

References

Brown, D.S., Nightingale, R.W., Alexander, D., Schrijver, C.J., Metcalf, T.R., Shine, R.A., Title, A.M., Wolfson, C.J.: 2003, *Solar Phys.* **216**, 79.
Canfield, R.C., Pevtsov, A.A.: 2000, *J. Astrophys. Astron.* **21**, 213.
Georgoulis, M.G., LaBonte, B.J.: 2004, *Astrophys. J.* **615**, 1029.
Ichimoto, K., Lites, B., Elmore, D., Suematsu, Y., Tsuneta, S., Katsukawa, Y., *et al.*: 2008, *Solar Phys.* **249**, 233.
Knoška, Š.: 1975, *Bull. Astron. Inst. Czechosl.* **26**, 151.
Kosugi, T., Matsuzaki, K., Sakao, T., Shimizu, T., Sone, Y., Tachikawa, S., *et al.*: 2007, *Solar Phys.* **243**, 3.
Leka, K.D., Canfield, R.C., McClymont, A.N., van Driel-Gesztelyi, L.: 1996, *Astrophys. J.* **462**, 547.
Li, H.: 2002, *Chin. J. Astron. Astrophys.* **2**, 174.
Linton, M.G., Longcope, D.W., Fisher, G.H.: 1996, *Astrophys. J.* **469**, 954.
Liu, J.H., Zhang, H.Q.: 2006, *Solar Phys.* **234**, 21.
Longcope, D.W., Klapper, I.: 1997, *Astrophys. J.* **488**, 443.
Longcope, D.W., Welsch, B.T.: 2000, *Astrophys. J.* **545**, 1089.
López Fuentes, M.C., Démoulin, P., Mandrini, C.H., Pevtsov, A.A., van Driel-Gesztelyi, L.: 2003, *Astron. Astrophys.* **397**, 305.
Low, B.C.: 1985, In: Hagyard, M.J. (ed.) *Measurements of Solar Vector Magnetic Fields* **NASA CP-2374**, 49.
Manchester, W.: 2001, *Astrophys. J.* **547**, 503.
Manchester, W., Gombosi, T., DeZeeuw, D., Fan, Y.: 2004, *Astrophys. J.* **610**, 588.
Metcalf, T.R., Jiao, L., McClymont, A.N., Canfield, R.C., Uitenbroek, H.: 1995, *Astrophys. J.* **439**, 474.
McClymont, A.N., Jiao, L.: 1997, *Solar Phys.* **174**, 191.
Molodenskii, M.M.: 1974, *Solar Phys.* **39**, 393.
Moon, Y.J., Choe, G.S., Yun, H.S., Park, Y.D., Mickey, D.L.: 2002, *Astrophys. J.* **568**, 422.
Parker, E.N.: 1979, *Astrophys. J.* **230**, 905.
Parker, E.N.: 1993, *Astrophys. J.* **408**, 707.

Priest, E.R.: 1984, *Solar Magneto-Hydrodynamics*, 18.
Scherrer, P.H., Bogart, R.S., Bush, R.I., Hoeksema, J.T., Kosovichev, A.G., Schou, J., *et al.*: 1995, *Solar Phys.* **162**, 129.
Shimizu, T.: 2004, *ASP Conf. Ser.* **325**, 2004.
Su, J.T., Zhang, H.Q.: 2007, *Astrophys. J.* **666**, 144.
Wang, H.M., Song, H., Jing, J., Yurchyshyn, V., Deng, Y.Y., Zhang, H.Q., Falconer, D., Li, J.: 2006, *Chin. J. Astron. Astrophys.* **4**, 477.
Zhang, H.Q., Wang, D.G., Deng, Y.Y., Hu, K.L., Su, J.T., Lin, J.B., *et al.*: 2007, *Chin. J. Astron. Astrophys.* **7**, 281.
Zhao, J.W., Kosovichev, A.G.: 2003, *Astrophys. J.* **591**, 446.